Composite fatigue failure of cold recycled material mixtures: new insights into the role of bitumen and cement

(Article begins on next page)

Composite fatigue failure of cold recycled material mixtures: new insights into the role of bitumen and cement

Andrea Graziani[a], Sara Spadoni[a], Lorenzo Paolo Ingrassia[a,*], Amedeo Virgili[a], Francesco Canestrari[a]

[a] Università Politecnica delle Marche, Via Brecce Bianche, 60131 Ancona, Italy

* Corresponding Author: l.p.ingrassia@pm.univpm.it

Abstract

In pavement engineering, cold recycled material (CRM) mixtures allow implementing circular economy concepts by maximizing the reuse of reclaimed asphalt without heating. Along with bitumen emulsion and foamed bitumen, Portland cement is often added to CRM mixtures to improve the field performance. However, the role of cement on the fatigue failure is not sufficiently investigated. The objective of this research is to provide new insights into the fatigue failure of CRM mixtures produced with bitumen emulsion and cement. To this aim, two CRM mixtures prepared with different dosages of cement (1% and 2%) were subjected to uniaxial cyclic tension fatigue tests. Empirical and energy-based failure criteria, originally developed for asphalt concrete mixtures, were used to define the fatigue failure. The results showed that the fatigue failure mechanism of CRM mixtures was of a composite type, affected by both cementitious and bituminous bonds. A new criterion was proposed to identify the failure of the cementitious bonds.

Keywords

Pavement; Cold recycling; Fatigue failure; Uniaxial test; Cement; Bitumen emulsion.

1. Introduction

Implementing circular economy concepts for achieving a sustainable development is a key goal of our society [1]. In pavement engineering, such concepts are put into practice by cold recycling technologies that allow reusing large amounts of reclaimed asphalt (RA) without heating. Compared to traditional hot mix asphalt (HMA) mixtures, cold recycled material (CRM) mixtures allow reducing greenhouse emissions and energy consumption [2][3][4][5]. Moreover, pavement structures containing courses built with CRM mixtures can have excellent long-term performance [6][7][8][9][10].

Among CRM mixtures, different families can be identified, depending on the type and amount of employed binding agents. Cement treated material (CTM) mixtures are produced if recycling is carried out by adding only Portland cement. Their load-related failure is normally due to fatigue [11][12]. If recycling is carried out by adding a small amount of bitumen (normally between 1.5% and 2.5%) bitumen stabilized materials (BSM) are produced. BSM are considered as improved granular materials and may include up to 1% Portland cement or other active fillers, like hydrated lime. The load-related failure of BSM is primarily due to permanent deformation [13][14]. Cement bitumen treated materials (CBTM) are produced with similar bitumen dosages but with higher dosages of Portland cement (normally between 1.5 and 4.0%). Load-related failure of CBTM is primarily due to fatigue [15][16][17].

The practical fatigue characterization of CRM mixtures has been routinely carried out in indirect tension configuration [16][17][18][19][20]. Some Authors have also performed cyclic bending tests on beam specimens [21][22][23]. The main limitation of those test configurations is that the stress-strain distribution within the specimen is not homogeneous [24]. A homogeneous stress-strain distribution is obtained with uniaxial tests on cylindrical specimens [25]. So far, only a couple of studies have characterized the fatigue behaviour of CRM mixtures through uniaxial tests [26][27]. It is readily apparent that very limited data are available in the literature, and none of these data refer to the case of CBTM mixtures.

Within this general context, the present research is part of a larger project that has the ultimate goal of evaluating the applicability of the viscoelastic continuum damage (VECD) theoretical-experimental framework to CRM mixtures. As a first necessary step, the objective of this paper is to provide new insights for understanding the fatigue failure of CRM mixtures. To this aim, two CRM mixtures produced with bitumen emulsion and different dosages of Portland cement were subjected to uniaxial cyclic tension fatigue tests. Empirical and energy-based failure criteria, originally developed for asphalt concrete (AC) mixtures, are used to define the fatigue failure. A fatigue failure mechanism that highlights the role of cement and a specific failure criterion are finally proposed.

2. Materials and methods

2.1 Materials

Two CRM mixtures, identified as CRM1 and CRM2, were investigated. Figure 1 shows their target gradation curve that was obtained by mixing 90 % of RA aggregate (RA 0/16) and 10 % of limestone filler [28]. The bitumen emulsion was a commercial cationic slow-setting type, modified with styrene-butadiene-rubber latex and designated C60BP10 according to EN 13808 [29]. For both mixtures, the dosage (by dry aggregate mass) of bitumen emulsion was 4.0 % (residual bitumen 2.4 %) and the total water content was 4.5 % (1.6 % bitumen emulsion water plus 2.9 % pre-wetting water).

The Portland cement was a type II/A LL, strength class 42.5 according to EN 197-1 [30]. Its dosages were 1.0 % and 2.0 % (by dry aggregate mass) for CRM1 and CRM2, respectively. CRM2 is a CBTM mixture typically produced in Europe for base and binder courses [31][32]. CRM1 may be considered a BSM and thus, in the field, its failure is expected to be caused by permanent deformation accumulation rather than fatigue. Nonetheless, it was included in the present experiment to verify if its fatigue failure characterization is possible.

The fatigue behaviour of the two CRM mixtures is compared to that of two typical AC mixtures for binder courses tested in a previous study [33]. One mixture (AC1) was produced with neat bitumen (PG 70-22) and the other (AC2) with styrene-butadiene-styrene (SBS) polymer modified bitumen (PG 82-16). The AC mixtures had similar aggregate gradations (dense graded, only virgin aggregates) and bitumen dosage of 4.5 % by mixture mass.

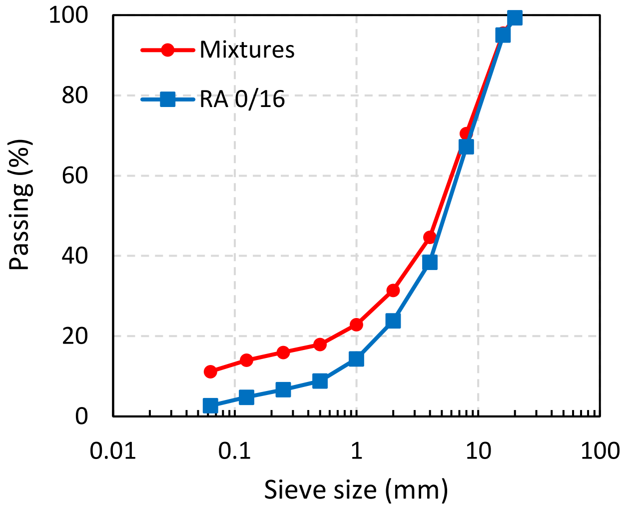

Figure 1. Gradation curves

2.2 CRM specimen preparation

The RA aggregate was initially dried at 40 °C, then the filler and part of the pre-wetting water (equal to the water absorption of the RA aggregate) were added and manually mixed. The wet blends were sealed in plastic bags for 12 h at room temperature to allow a uniform moisture distribution. Afterwards, the cement, the remaining pre-wetting water and the bitumen emulsion were gradually added and mixed, alternating manual and mechanical mixing [34].

From each mixture batch, one cylindrical specimen was prepared using a gyratory compactor with vertical pressure of 600 kPa, rotation speed of 30 rpm and external angle of inclination of 1.25° [35]. In total, ten specimens with diameter of 150 mm and height of 180 mm were compacted at the target voids content of 14.0 % (five from CRM1 and five from CRM2). It is worth noting that voids of readily compacted CRM mixtures include the volume of air and intergranular water [36]. All specimens were extracted from the mould immediately after compaction.

A two-stage curing procedure was adopted. The gyratory specimens were cured for one day in the oven at 40 °C (dry environment), and then enclosed in plastic bags and cured until 28 days in a climatic chamber at 40 °C (moist environment). In the first stage, the curing of the bituminous binder is facilitated thanks to the moisture loss due to evaporation, whereas in the second stage the hydration of the cementitious binder is promoted using the residual water present in the mixture [37]. This procedure was adopted because is somewhat similar to what happens in the field, where free evaporation from the surface of the CRM layer is allowed for some hours or days, until the upper layer is constructed.

After the 28 curing days, one test specimen with diameter of 100 mm and height of 130 mm was cored and cut from the inner part of each gyratory sample. The bulk density of the cored specimens was obtained with the hydrostatic method [38] and then the air void content was calculated according to EN 12697-8 [39]. The average (standard deviation) value of air void content was 12.7 % (0.6 %) for CRM1 and 12.6 % (0.6 %) for CRM2.

The AC mixtures were produced in an asphalt plant, reheated and compacted in the laboratory using a gyratory compactor [33]. The compacted samples had diameter of 150 mm, height of 170 mm and target air void content of 5.0 % for the inner portion of the sample. Afterwards, four “small” test specimens with diameter of 38 mm and height of 110 mm were cored and cut from each gyratory sample, in accordance with AASHTO PP 99 [40]. The average (standard deviation) value of air void content was 5.3 % (0.4 %) for AC1 test specimens and 5.2 % (0.1 %) for AC2 test specimens.

It is worth underlining that, since this was one of the first experiences ever concerning axial fatigue testing of CRM mixtures, the adoption of the small geometry (38 mm diameter, 110 mm height) was deemed premature by the Authors. Therefore, the large specimen geometry suggested by AASHTO T 400 (100 mm diameter, 130 mm height) was considered for the CRM mixtures as a first step.

2.3 Complex modulus and cyclic fatigue testing

The testing procedure followed for the CRM mixtures is standardized by AASHTO T 400 [41] for conventional AC mixtures to obtain the damage characteristic curve within the VECD theoretical-experimental approach. This procedure includes cyclic tension-compression stiffness tests and cyclic tension fatigue tests carried out with the Asphalt Mixture Performance Tester (AMPT), using the setup shown in Figure 2a. Loading platens are glued to the top and bottom of the specimens with an epoxy adhesive. Three axial LVDTs are mounted approximately 120° apart in order to measure the axial strain in the central 70 mm of the specimen. The fatigue tests are performed in constant crosshead mode. Compared to strain-controlled tests, crosshead-controlled tests are easier to run and reduce the risk of damaging the equipment if improperly performed [42]. As an example, Figure 2b shows the typical stress and strain signals at the beginning of the test for an AC mixture (the actuator strain is obtained as the ratio between the actuator displacement and the specimen height). The applied sinusoidal axial load is adjusted to keep the actuator displacement amplitude constant throughout the test. Even though the on-specimen strain remains tensile, both tensile and compressive stresses are applied on the specimen due to viscous effects. The actual on-specimen strain is lower than the actuator strain level due to inevitable machine compliance issues. The test is stopped when the machine is no longer able to apply a well-shaped sinusoidal load.

On CRM specimens, the complex modulus test (also known as fingerprint test) was performed at 20 °C and 10 Hz to evaluate the linear viscoelastic properties of each specimen. The test consisted in applying 55 cycles of a sinusoidal tension-compression axial load adjusted to achieve a target peak-to-peak on-specimen strain amplitude between 25 and 35 microstrain, which is a typical strain value to observe a linear behaviour [43][44]. After a rest period of 5 minutes, the cyclic fatigue test was performed at the same temperature and frequency. The initial peak-to-peak on-specimen tensile strain amplitude ($\varepsilon_{0,initial}$) was selected between 70 and 80 microstrain, which led to test durations between 2000 and 60000 cycles.

For the AC mixtures the testing temperature and frequency were 21 °C and 10 Hz. The target strain amplitude was between 50 and 75 microstrain in the fingerprint test, and $\varepsilon_{0,initial}$ was between 380 and 450 microstrain in the fatigue test, which led to test durations between 2000 and 80000 cycles [33].

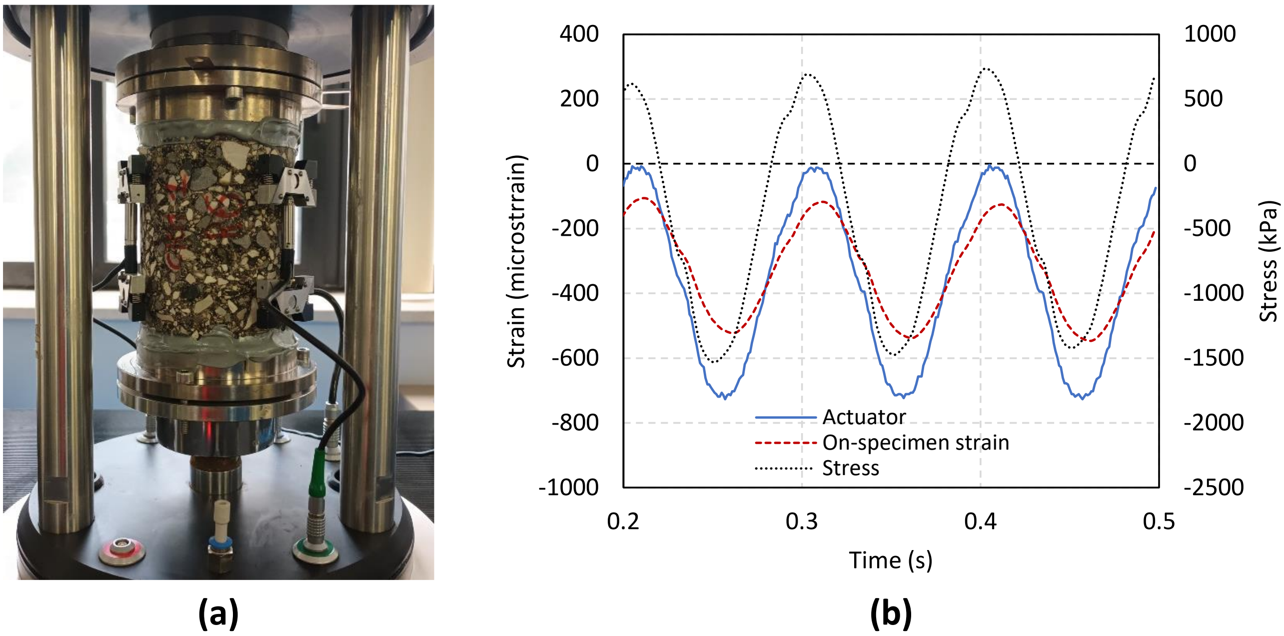

Figure 2. Testing: (a) setup for complex modulus and cyclic fatigue tests, (b) stress and strain at the beginning of the fatigue test (in the figure, tension is negative while compression is positive)

2.4 Examined fatigue failure criteria

Fatigue failure criteria that have been developed for AC mixtures can be grouped into two main categories: empirical and energy-based [45][46][47][48].

The most common empirical criterion consists in arbitrarily defining the specimen failure based on the 50 % reduction of the initial stiffness modulus [49][50]. Another common empirical criterion is based on the observation of the phase angle evolution that typically shows an increase followed by a sharp drop. It is assumed that the maximum phase angle corresponds to the formation of macrocracks, and thus to the specimen failure [51].

Energy-based failure criteria rely on the calculation of the dissipated energy per unit volume per cycle (W), i.e., the area of the stress-strain hysteresis loop, using the following linear approximation:

$$W = \pi \cdot \sigma \cdot \varepsilon \cdot \sin\delta = \pi \cdot \varepsilon^2 \cdot E \cdot \sin\delta \tag{1}$$

where σ is the stress amplitude, ε is the strain amplitude, E is the stiffness modulus and δ is the phase angle at a given cycle.

Pronk and Hopman [52] introduced the dissipated energy ratio (DER) parameter to identify the fatigue failure, based on the previous work by Van Dijk [53] and Van Dijk and Visser [54]. DER is defined as the ratio between the total cumulated dissipated energy up to cycle n and the dissipated energy at cycle n:

$$DER = \frac{\sum_{i=1}^{n} W_i}{W_n} \tag{2}$$

The relationship between DER and number of load cycles follows the line of equality (slope equal to 1) when the specimen is undamaged. As damage develops, the DER curve progressively bends upwards (strain-controlled tests) or downwards (stress-controlled tests).

The criterion currently adopted by the reference standard AASHTO T 400 [41] is the so-called stress degradation ratio criterion, which is a simplification of the DER criterion. Fatigue failure is identified by the peak value of the product of stress amplitude and cycle number ($\sigma \cdot N$). The main advantage of this criterion is that phase angle measurement is not needed.

The abovementioned criteria, typically adopted for traditional AC mixtures, were applied to the investigated CRM mixtures.

3. Results and analysis

3.1 Complex modulus results

Figure 3 summarizes the results of the complex modulus fingerprint tests in terms of stiffness modulus and phase angle. The average (standard deviation) values of the stiffness modulus were 4496 MPa (572 MPa) and 7050 MPa (453 MPa) for CRM1 and CRM2, respectively. Instead, the average (standard deviation) values of the phase angle were 9.1° (0.7 °) and 6.9 ° (0.4 °) for CRM1 and CRM2, respectively. Such differences are statistically significant and were expected due to the higher cement content of CRM2 with respect to CRM1 (2 % vs 1 %).

Figure 3 also summarizes the results observed for the AC mixtures. The average (standard deviation) values of the stiffness modulus were 6755 MPa (298 MPa) and 7671 MPa (484 MPa) for AC1 and AC2, respectively. Instead, the average (standard deviation) values of the phase angle were 21.9° (0.7°) and 21.8° (0.4°) for AC1 and AC2, respectively.

The main difference between the CRM and AC mixtures lies in the phase angle values, which were significantly higher for the AC mixtures. This expected difference denotes a more pronounced dissipation behaviour for AC mixtures with respect to the CRM mixtures (especially CRM2).

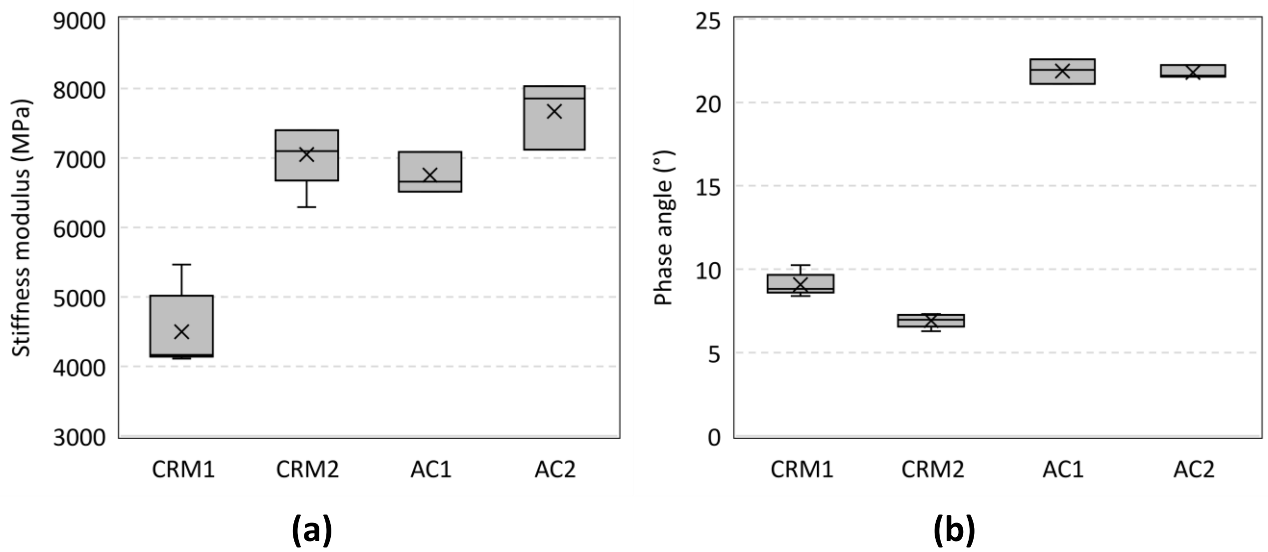

Figure 3. Complex modulus results: (a) stiffness modulus, (b) phase angle

3.2 Evolution of stress and strain during the fatigue test

Figure 4a shows the evolution of stress and on-specimen strain during the fatigue test for representative specimens of CRM1 (specimen R15, $\varepsilon_{0,initial}$ = 75 microstrain) and CRM2 (specimen R1, $\varepsilon_{0,initial}$ = 80 microstrain). For comparison purposes, Figure 4c shows the same data for representative specimens of AC1 (specimen #3, $\varepsilon_{0,initial}$ = 380 microstrain) and AC2 (specimen #3, $\varepsilon_{0,initial}$ = 450 microstrain). In these figures, both stress and strain are normalised with respect to their initial value. In addition, Figure 4b and Figure 4d show the evolution of the mode factor (MF) defined by Monismith and Deacon [55]:

$$MF = \frac{|A| - |B|}{|A| + |B|} \tag{3}$$

where $|A|$ and $|B|$ are the percentage variation in stress and strain, respectively, for an arbitrary but fixed reduction in mixture stiffness. MF is equal to – 1 for purely stress-controlled tests and + 1 for purely strain-controlled tests.

Figure 4a shows the different behaviour of mixtures CRM1 and CRM2. All CRM1 specimens (plus one CRM2 specimen) exhibited a progressive stress decrease and strain increase until reaching a sub-horizontal asymptote. Instead, for most CRM2 specimens (4 out of 5), both stress and strain followed a S-shape evolution during the test. For the AC mixtures (Figure 4c), the stress reduced rapidly while the strain increased rapidly in the very first phase of the test, then the stress decreased while the strain increased in a steady quasi-linear manner in the second phase, and finally the stress rapidly decreased and the strain rapidly increased in the third phase.

Figure 4a and Figure 4c confirm that the test is neither in stress control mode (constant stress) nor in strain control mode (constant strain). For the selected representative specimens, the MF values oscillated between – 0.7 and – 1 for the CRM mixtures, and between 0 and – 0.5 for the AC mixtures.

In fact, for the CRM mixtures, the strain variation was predominant over the stress variation and the test was almost in stress control mode, especially for CRM2 specimens with higher cement content (MF ≈ −1). For the AC mixtures, the test can be considered in mixed mode of loading, even though the strain variation was still predominant over the stress variation (MF < 0).

It can be concluded that the test was more severe for CRM mixtures than for conventional AC mixtures. Moreover, the common fatigue failure criteria that are employed in the case of constant stress or constant strain may not be applicable, especially for CRM mixtures.

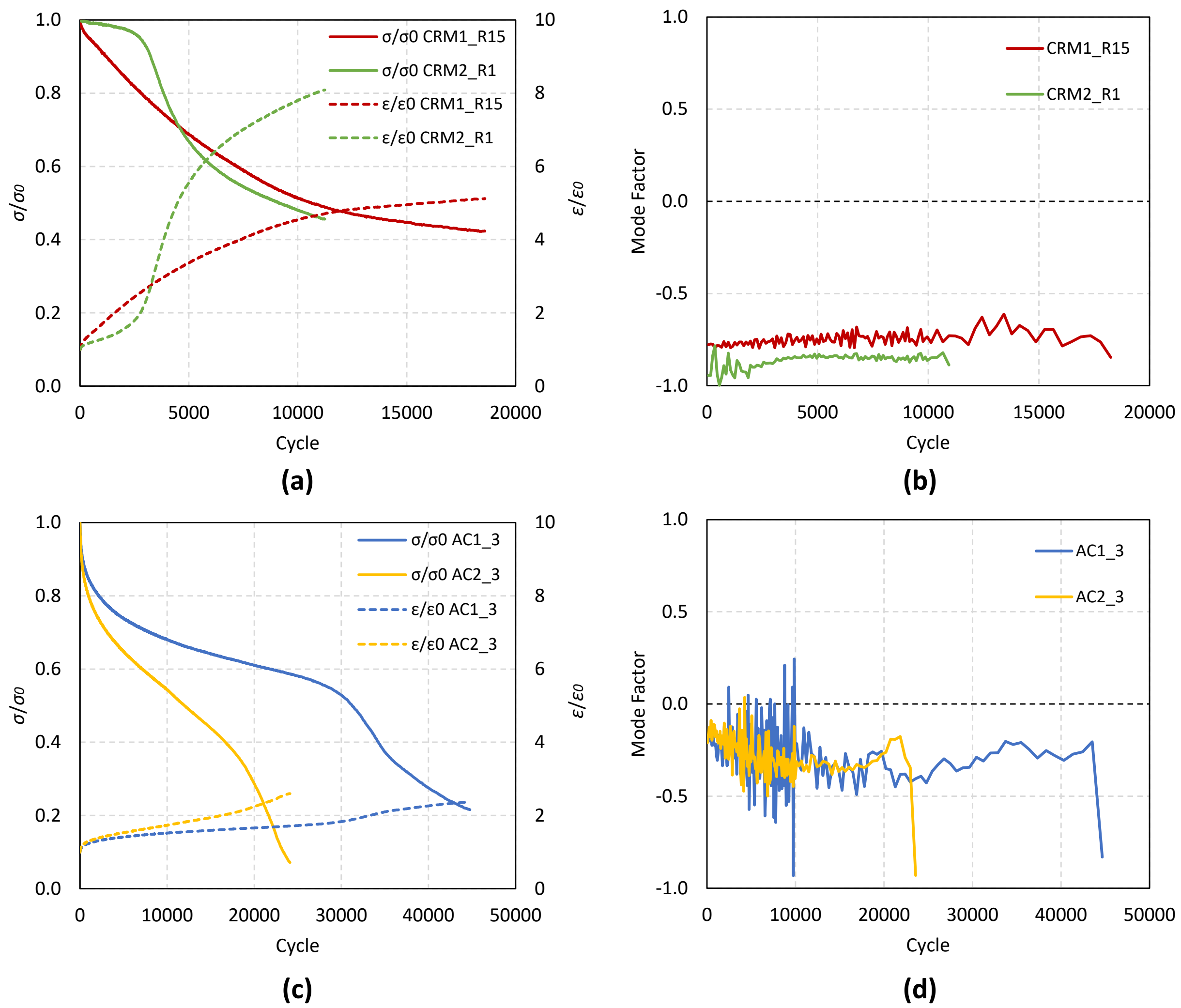

Figure 4. Evolution of: (a) stress and strain and (b) mode factor for CRM1 and CRM2; (c) stress and strain and (d) mode factor for AC1 and AC2

3.3 Empirical fatigue failure criteria

Figure 5 shows the evolution of stiffness modulus and phase angle (both normalised with respect to the initial value) during the fatigue test for the same four representative specimens shown above.

For the AC mixtures (Figure 5b), the three typical phases can be identified [48][56]. In the initial loading cycles (adaptation phase) the stiffness reduces rapidly while the phase angle increases rapidly due to the combined effect of fatigue damage, heat development and thixotropy. In the second phase (quasi-stationary phase) the stiffness keeps decreasing while the phase angle keeps increasing, both with a steady quasi-linear trend. This behaviour is normally associated with the development of damage due to the formation of microcracks. This second phase ends with an inflection point that denotes the beginning of the transition towards the third phase (failure phase), which is characterised by a fast decrease in stiffness and phase angle and is associated with the formation and propagation of macrocracks leading to the specimen physical failure.

The evolution of stiffness modulus and phase angle was similar between CRM1 and CRM2 mixtures, but different from the one described above (Figure 5a). Specifically: a) in both the stiffness and phase angle curves the quasi-stationary phase was not present; b) the phase angle evolution showed a sharper maximum value (the maximum δ/δ_0 value was around 1.5 for the AC specimens, higher than 2.0 for the CRM2 specimens and intermediate for the CRM1 specimens); c) the stiffness modulus curves were characterized by a relatively long and almost flat final part (without the inflection point that typically denotes the transition between the second and third phases for AC mixtures). This behaviour suggests different fatigue damage mechanisms for CRM mixtures, as compared to traditional AC mixtures.

Figure 5 also shows the fatigue failure points identified using the two most common empirical criteria: 50 % reduction in the stiffness modulus ($N_{f,E}$) and maximum phase angle ($N_{f,\delta}$). Table 1 summarizes the values of $N_{f,E}$ and $N_{f,\delta}$, along with the ratio $N_{f,\delta}$ / $N_{f,E}$ and the normalised value of the stiffness modulus at the number of cycles $N_{f,\delta}$.

For all specimens, $N_{f,\delta}$ is higher than $N_{f,E}$. However, the $N_{f,\delta}$ / $N_{f,E}$ ratio is generally lower for CRM mixtures (especially CRM2) as compared to AC mixtures, indicating that $N_{f,\delta}$ is closer to $N_{f,E}$ for CRM mixtures. Nevertheless, it should be recalled that CRM and AC specimens were tested at significantly different strain levels (see the values of $\varepsilon_{0,initial}$ in Table 1). An interesting common feature between CRM and AC mixtures is that the maximum phase angle broadly occurs when the stiffness modulus is approximately 20 % of the initial value E_0, as denoted by the values of E/E_0 @ $N_{f,\delta}$ in Table 1.

The $N_{f,E}$ and $N_{f,\delta}$ values are plotted in Figure 6. In particular, the data related to the two ACs are plotted together as a single data set, because AC1 and AC2 exhibited the same macroscopic behaviour. Figure 6 clearly highlights that the maximum phase angle criterion leads to higher N_f values with respect to the 50 % modulus reduction criterion. The parameters of the fitting lines in Figure 6 ($\log N_{f,E} = a \log N_{f,\delta} + b$) were determined using the total least square (TLS) method, and the correlation between $N_{f,E}$ and $N_{f,\delta}$ was assessed through the Pearson coefficient ρ. The values of the parameters a and b summarized in Table 2 indicate that the slope of the fitting function is somewhat similar for CRM1 and AC, whereas it is considerably different for CRM2 with higher cement content. Moreover, the Pearson coefficients denote a good correlation between $N_{f,E}$ and $N_{f,\delta}$ for CRM2 and AC ($\rho > 0.70$) and a moderate correlation for CRM1 ($\rho = 0.61$).

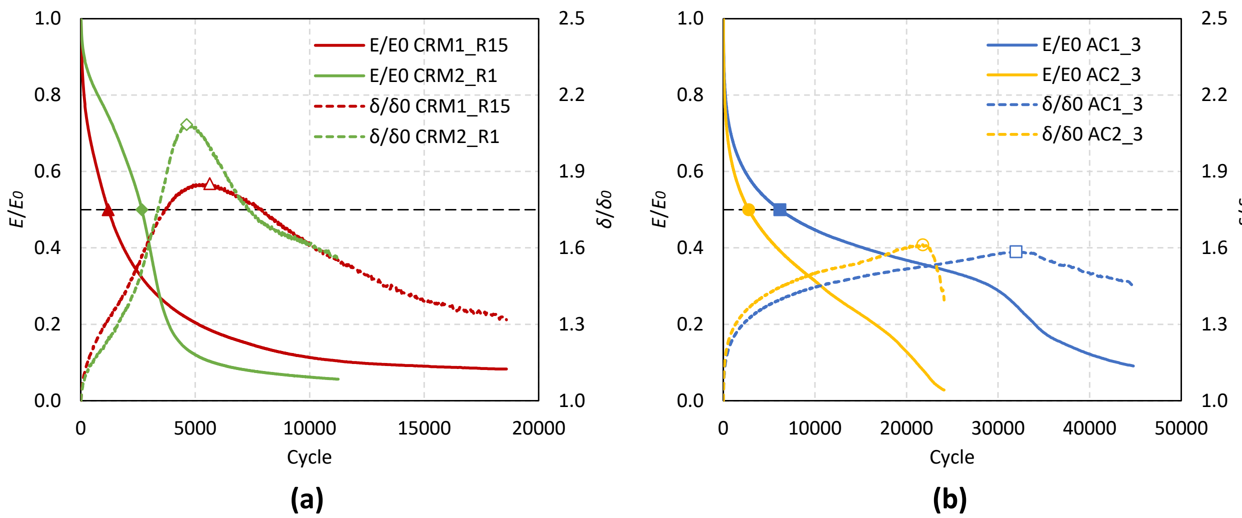

Figure 5. Evolution of stiffness modulus and phase angle for (a) CRM1 and CRM2, (b) AC1 and AC2

Table 1. Number of cycles to failure determined according to the empirical failure criteria

Mixture	Specimen	$\varepsilon_{0,initial}$ (microstrain)	$N_{f,E}$	$N_{f,\delta}$	$N_{f,\delta}$ / $N_{f,E}$	E/E_0 @ $N_{f,\delta}$
CRM1	R5	80	3550	7280	2.1	0.34
	R14	70	4460	46900	10.5	0.12
	R15	75	1200	5630	4.7	0.19
	R17	75	1710	6720	3.9	0.24
	R18	70	8040	28040	3.5	0.27
	Average				*3.7*	*0.23*
CRM2	R1	80	2670	4630	1.7	0.14
	R5	80	760	2130	2.8	0.18
	R9	75	510	1460	2.9	0.14
	R10	75	2040	11140	5.5	0.18
	R11	75	9500	14170	1.5	0.17
	Average				*2.3*	*0.16*
AC1	1	400	3640	12790	3.5	0.23
	2	430	2110	9420	4.5	0.08
	3	380	6170	31950	5.2	0.25
	Average				*4.3*	*0.19*
AC2	1	400	4830	39710	8.2	0.27
	2	430	3310	12470	3.8	0.17
	3	450	2760	21770	7.9	0.08
	Average				*5.8*	*0.17*

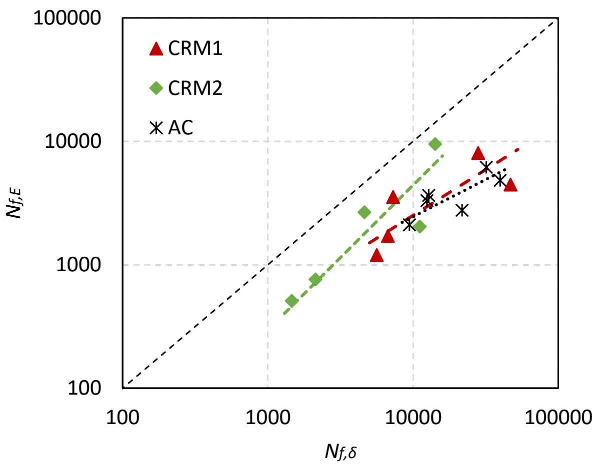

Figure 6. $N_{f,E}$ vs $N_{f,\delta}$

Table 2. Fitting line parameters and Pearson coefficient for the data sets in Figure 6

Mixture	Slope (a)	Intercept (b)	Correlation (ρ)
CRM1	0.74	0.43	0.61
CRM2	1.17	–1.05	0.82
AC	0.60	0.98	0.77

3.4 Energy-based fatigue failure criteria

Figure 7 shows the evolution of the stress degradation ratio parameter ($\sigma{\cdot}N$) for the same four representative specimens shown above. The fatigue failure points corresponding to the maximum $\sigma{\cdot}N$ value ($N_{f,\sigma{\cdot}N}$) and to the maximum phase angle ($N_{f,\delta}$) are also highlighted in the figure. Note that, in the two subfigures, the scale on the y-axis is different (the AC specimens showed significantly higher values).

The AC specimens showed the expected behaviour, i.e., the parameter $\sigma{\cdot}N$ increased during the test until reaching its maximum value and then dropped rapidly before the specimen collapse. It is also worth noting that $N_{f,\sigma{\cdot}N}$ slightly precedes $N_{f,\delta}$, in agreement with the literature [57]. Conversely, for the CRM specimens, the parameter $\sigma{\cdot}N$ steadily increased until the specimen collapse, confirming the different fatigue damage mechanisms with respect to AC mixtures. More in detail, the parameter $\sigma{\cdot}N$ increased at a higher rate in the first part of the test, and at a slower rate in the second part of the test, suggesting that the physical mechanism leading to energy dissipation changed as damage increased during the test. The absence of a peak value in the $\sigma{\cdot}N$ curve was expected because the test is almost in pure stress control mode for the CRM mixtures, as shown in Figure 4b ($\sigma \cdot N = f(N)$ is a line with slope equal to σ for a purely stress-controlled test). $N_{f,\delta}$ broadly corresponded to the beginning of the second phase, characterized by a slower increase of the parameter $\sigma{\cdot}N$.

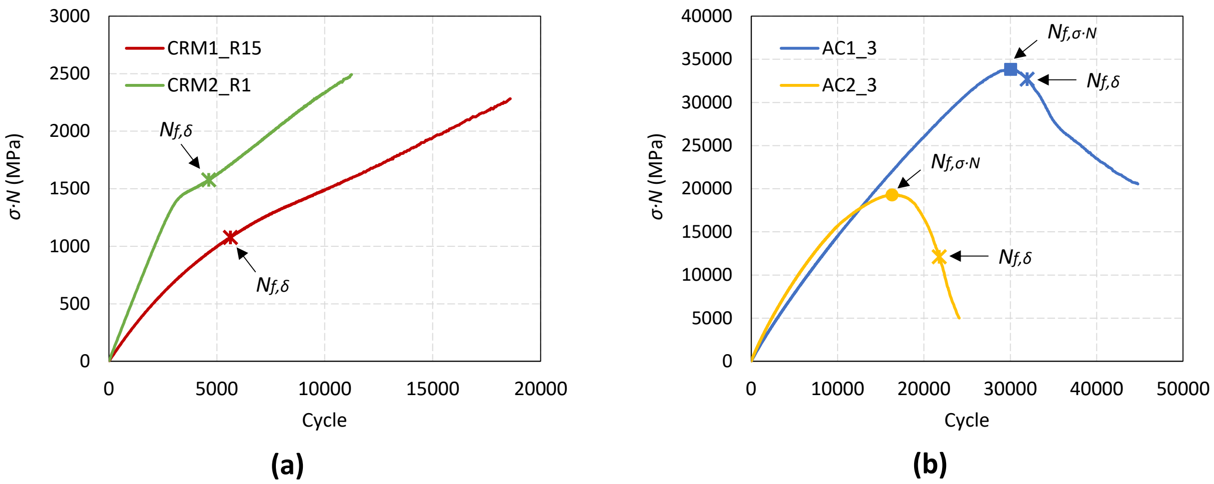

Figure 7. Evolution of the parameter $\sigma{\cdot}N$ for (a) CRM1 and CRM2, (b) AC1 and AC2

Since the point of maximum for $\sigma{\cdot}N$ cannot be used to define fatigue failure, it is necessary to take a step back and examine first the evolution of the dissipated energy per unit volume per cycle (Equation 1) during the test.

Figure 8 shows the evolution of W for the same four representative specimens shown above. It should be noted that W was one order of magnitude higher for the AC mixtures, which was expected, given the higher applied strain level and phase angle with respect to CRM mixtures (Figure 5, Table 1). The fatigue failure point corresponding to the maximum phase angle ($N_{f,\delta}$) is also highlighted in the figure.

For AC specimens, the dissipated energy increased rapidly in the very first loading cycles, then remained almost constant in the central part of the test, before dropping very quickly in the final part (Figure 8b). The three typical phases that characterize the evolution of modulus and phase angle (Figure 5b) can be easily recognised. Moreover, Figure 8b shows that $N_{f,\delta}$ corresponds to the end of the constant phase for specimen AC1_3, whereas it is located in the descending part of the curve for specimen AC2_3.

Conversely, for CRM specimens, the dissipated energy increased in the first part of the test until reaching a maximum, and then decreased at a slower rate compared to the first part until the end of the test (Figure 8a). This behaviour is more evident for CRM2 with respect to CRM1. As highlighted above, the quasi-stationary phase that characterizes damage evolution in AC mixtures is completely missing. On the other hand, such an evolution (increasing in the first part, decreasing in the second part) confirms that the energy dissipation mechanism changed during the test. It should be also noted that, for both CRM1 and CRM2 specimens, the maximum phase angle almost corresponded to the maximum value of W. In addition, the CRM2 curve is characterized by two evident inflection points, one before and one after the peak W value. In the case of CRM1, only the inflection point after the peak W value is immediately apparent.

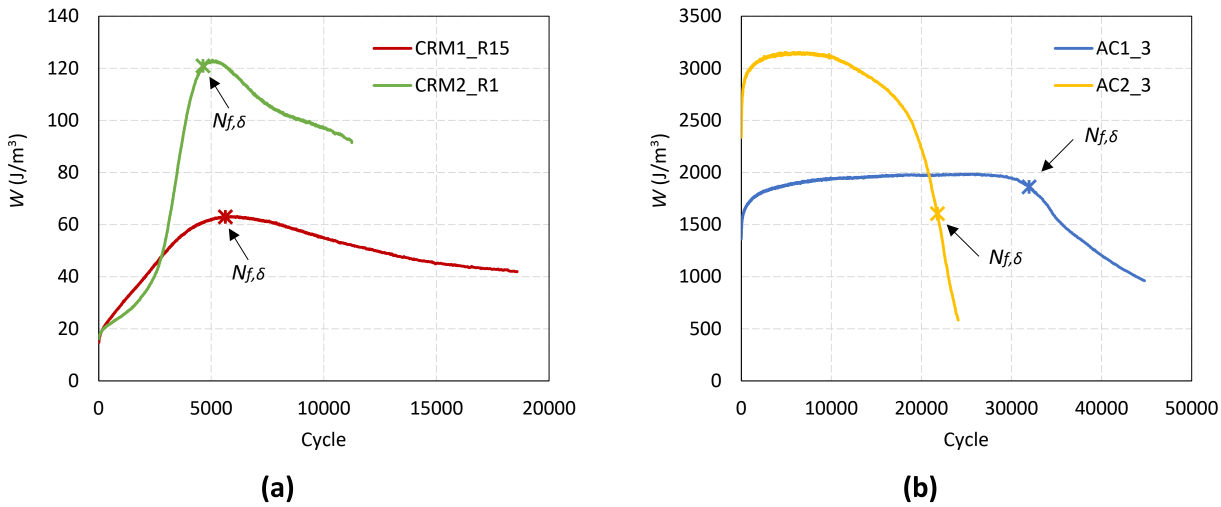

Figure 8. Evolution of the dissipated energy per unit volume per cycle for (a) CRM1 and CRM2, (b) AC1 and AC2

The differences in the dissipated energy per cycle led to a different evolution of the DER (Figure 9). For the CRM specimens, a zoom of the initial part of the test is presented in Figure 9a, as these are the data of greatest interest.

Figure 9b shows the typical DER evolution that characterizes AC mixtures in a strain-controlled test (MF indicates that the test is in mixed mode of loading, see Figure 4). As long as the specimen is undamaged, the DER curve is superimposed to the line of equality, then the curve progressively deviates, approaching an oblique asymptote (irrecoverable fatigue asymptote). One way to define the number of cycles to failure based on the DER curve is to consider the intersection between the no damage line and the irrecoverable fatigue asymptote, as shown in Figure 9b.

Figure 9a shows that the behaviour of CRM mixtures was totally different. First, the DER values are located below the line of equality from the very early testing cycles. This behaviour typically characterizes damage in stress-controlled tests (the MF is indeed close to –1, see Figure 4). Second, the DER evolution of CRM2 specimens showed a local maximum, an inflection point (highlighted in Figure 9a), and a local minimum within a relatively short interval of cycles. After the local minimum, the DER value increased again at a rather constant rate until the specimen failure (not shown in the plot). For CRM1, such a behaviour was less pronounced, but an inflection point is present also in this case (as highlighted in Figure 9a). A possible interpretation of the fatigue failure mechanism of CRM mixtures is proposed in the next section.

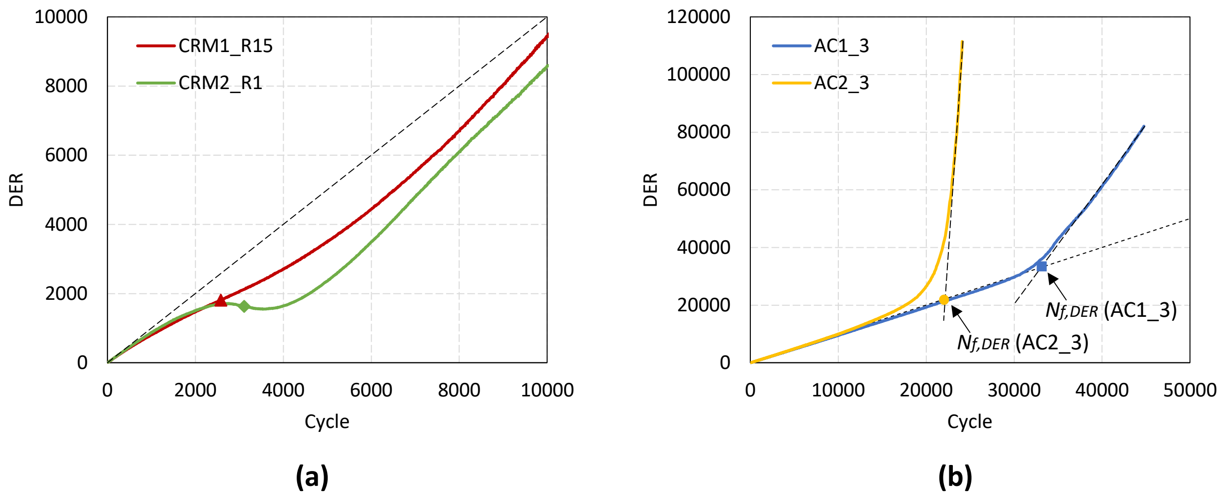

Figure 9. Evolution of DER for (a) CRM1 and CRM2, (b) AC1 and AC2

4. Discussion

4.1 Interpretation of the composite fatigue failure of CRM specimens

The experimental results clearly showed that the fatigue damage evolution of CRM and AC specimens was different. It is readily apparent that such a difference was due to the presence of cementitious bonds, and the different behaviour between CRM1 and CRM2 mixtures also confirms that the cement dosage played a critical role. Consequently, a different fatigue failure criterion, specifically devoted to identifying the composite effect of cementitious and bituminous bonds is necessary.

A possible interpretation of the fatigue failure of CRM specimens is outlined in Figure 10. At the beginning of the fatigue test, the cementitious bonds carried most of the applied tensile load due to their higher stiffness with respect to the bituminous bonds. However, they are also more brittle than the bituminous bonds and thus started failing as the tensile strain amplitude increased in the first stage of the test (Figure 4 and Figure 8). We suggest that the local maximum, the inflection point, and the local minimum that characterize the initial DER evolution for CRM2 specimens (Figure 9a) were due to the failure of the cementitious bonds.

The local failure of the cementitious bonds can be interpreted as microcracks that reduce the effective area of the specimen. Those microcracks could originate from the breaking of the cement hydrates or from a detachment at the interface between the hydrates and the aggregate particles, mostly composed of RA particles. Failure of the cementitious bonds started at a relatively low number of loading cycles and extended through a narrow interval of cycles. The process led to the dramatic reduction of stiffness and increase in phase angle shown in Figure 5a, as the stress was progressively transferred to the bituminous binder. This explains the observed dramatic increase of dissipated energy per cycle (Equation 1, Figure 8a), which in turn causes the decrease of DER (Equation 2, Figure 9a). It is important to note that, at this stage, the formation of macrocracks can be reasonably excluded because they would lead to the specimen collapse within a few cycles. As the number of loading cycles further increased, the bituminous bonds progressively carried a higher share of the load, and therefore they were also affected by an increasing damage. We observe a decreasing trend of the dissipated energy per cycle and the DER curve starts increasing again (slope greater than 1). Such a behaviour is similar to that of conventional AC mixtures in strain-controlled tests and ultimately leads to the development of macrocracks, followed by the specimen collapse.

The damage evolution for CRM1 specimens was characterised by smoother transitions in the evolution of energy dissipation (Figures 8a and 9a), highlighting the lower impact of the cementitious bonds, which is clearly due to the lower cement dosage.

Overall, the evolutions of both *W* and DER suggest that for CRM mixtures there was a transition from a cement-dominated to a bitumen-dominated dissipation behaviour and that the fatigue failure was a composite phenomenon affected by both cementitious and bituminous bonds.

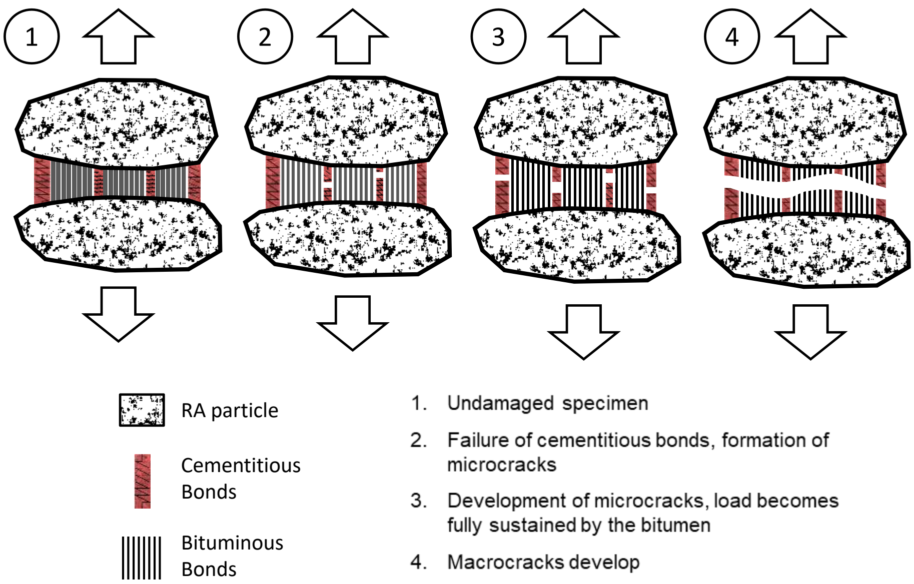

Figure 10. Interpretation of fatigue failure of CRM specimens

4.2 Fatigue failure criterion for CRM specimens

We suggest that, for CRM mixtures, the inflection point of the DER evolution curve (highlighted in Figure 9a) can be used to identify the number of cycles corresponding to the failure of the cementitious bonds. The inflection point can be calculated using several numerical procedures. In this research we applied the algorithm developed by Virgili et al. [58] to identify the failure point of reinforced double-layered asphalt specimens in cyclic four-point bending tests.

Table 3 reports the number of cycles to failure $N_{f,DER}$ corresponding to the inflection point of the DER evolution curve for all CRM specimens. For AC specimens, failure was identified with the tangent intersection method (Figure 9b). Figure 11 compares the $N_{f,DER}$ values with the number of cycles to failure determined according to the 50 % modulus reduction criterion ($N_{f,E}$) and the maximum phase angle criterion ($N_{f,\delta}$).

For all specimens, the $N_{f,DER}$ / $N_{f,E}$ ratio was higher than one, and higher values were obtained for the AC mixtures with respect to the CRM mixtures (Figure 11a). Once again, it is highlighted that the 50 % modulus reduction is an arbitrary failure definition without any direct physical interpretation.

For AC specimens, the $N_{f,DER}$ / $N_{f,\delta}$ ratio is comprised between 1.0 and 1.56 (average value of 1.18, standard deviation of 0.24). It has been reported by several Authors that for AC mixtures the DER criterion and the maximum phase angle criterion are almost equivalent [47][59]. For CRM specimens, the $N_{f,DER}$ / $N_{f,\delta}$ ratio is comprised between 0.33 and 1.05 (average value of 0.67, standard deviation of 0.23). These values suggest that the two criteria describe different failure mechanisms. Specifically, $N_{f,DER}$ could identify the failure of the cementitious bonds, whereas $N_{f,\delta}$ could identify the failure of the bituminous bonds, analogously to AC mixtures. The parameters of the fitting lines in Figure 11b ($N_{f,DER}$ vs $N_{f,\delta}$) are shown in Table 4 and indicate that also in this case the fitting functions are somewhat similar for CRM1 and AC (in particular, they are parallel with slope approximately equal to 1), whereas the slope of the fitting line for CRM2 is considerably different. The Pearson coefficients indicate a good correlation between $N_{f,DER}$ and $N_{f,\delta}$ for all mixtures ($\rho > 0.70$).

Finally, we remark that both the DER-based criterion (failure of cementitious bonds) and the maximum phase angle criterion (failure of bituminous bonds) highlighted a longer fatigue life for CRM1 with respect to CRM2. However, as long as field behaviour is concerned, typically CRM mixtures produced with 1% Portland cement (or less) are not prone to fatigue because permanent deformation accumulation is more severe. On the other hand, if Portland cement dosage is equal to or greater than 2%, permanent deformation is normally not an issue [20]. It should also be noted that, beyond the point of maximum phase angle, all CRM specimens were characterized by a relatively long life before collapse (Figure 5a). During this phase, stiffness is quite low (less than 20 % of the initial value), but phase angle is rather high and, overall, this led to values of dissipated energy per cycle that were higher than those measured in the undamaged specimens (Figure 8a). This aspect, that must be further investigated, may affect the field behaviour of CRM mixtures.

Table 3. Number of cycles to failure determined according to the proposed energy-based failure criterion and comparison with the empirical failure criteria

Mixture	Specimen	$N_{f,DER}$	$N_{f,DER}$ / $N_{f,E}$	$N_{f,DER}$ / $N_{f,\delta}$
CRM1	R5	5178	1.46	0.71
	R14	17466	3.92	0.37
	R15	2578	2.15	0.46
	R17	4290	2.51	0.64
	R18	29562	3.68	1.05
	Average		*2.74*	*0.65*
CRM2	R1	3108	1.16	0.67
	R5	1573	2.07	0.74
	R9	1246	2.44	0.85
	R10	3712	1.82	0.33
	R11	11776	1.24	0.83
	Average		*1.75*	*0.68*
AC1	1	20000	5.49	1.56
	2	9400	4.45	1.00
	3	32000	5.19	1.00
	Average		*5.05*	*1.19*
AC2	1	56000	11.59	1.41
	2	14000	4.23	1.12
	3	22000	7.97	1.01
	Average		*7.93*	*1.18*

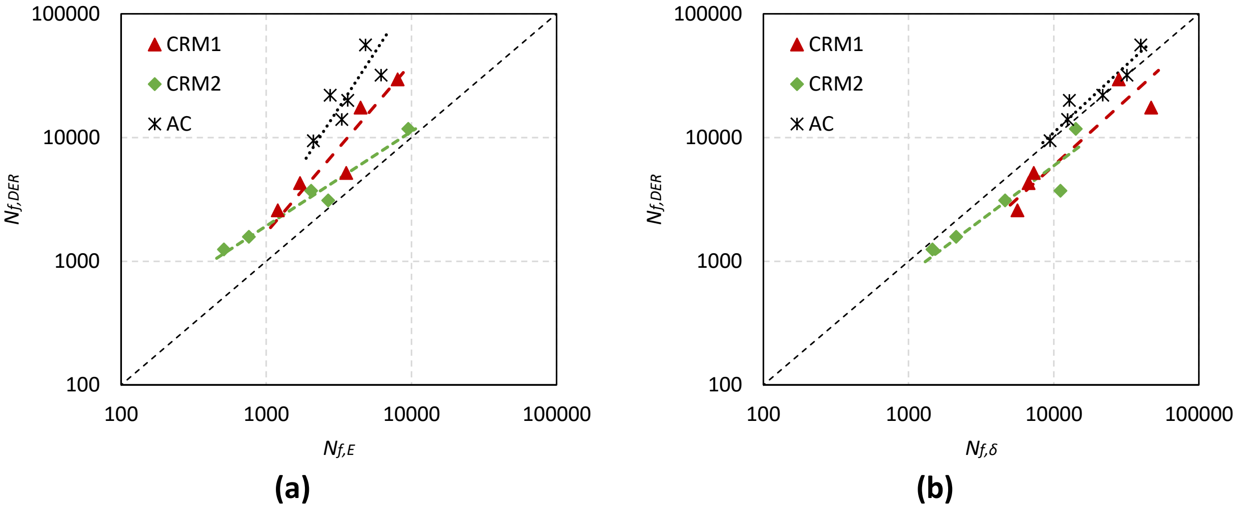

Figure 11. $N_{f,DER}$ vs (a) $N_{f,E}$, (b) $N_{f,\delta}$

Table 4. Fitting line parameters and Pearson coefficient for the data sets in Figure 11b

Mixture	Slope (*a*)	Intercept (*b*)	Correlation (*ρ*)
CRM1	1.07	–0.49	0.73
CRM2	0.88	0.27	0.86
AC	1.09	–0.32	0.95

5. Conclusions

The objective of this research was to provide new insights into the fatigue failure of CRM mixtures. To this aim, two CRM mixtures characterized by different dosages of Portland cement (1% and 2%), were subjected to uniaxial cyclic tension fatigue tests in control crosshead mode. Empirical and energy-based failure criteria typically adopted for AC mixtures were applied to analyse the results, and the main findings can be summarized as follows:

- The stress/strain evolution during the fatigue test highlighted that the test was almost in pure stress control mode for the CRM mixtures whereas it was in mixed mode for the AC mixtures. Hence the test was more severe for CRM mixtures.

- The stiffness modulus and phase angle evolution of CRM mixtures were characterized by: a) the absence of the quasi-stationary phase; b) a sharper maximum value of the phase angle curve; c) a relatively long and almost flat final part of the stiffness modulus curves.
- The energy dissipation evolution of CRM mixtures was characterised by: a) the absence of a peak in the evolution of the parameter $\sigma \cdot N$; b) the rapid increase of the dissipated energy per cycle until reaching a maximum, followed by a slower decrease until the end of the test; c) the DER curve was below the equality line from the very early testing cycles and showed an inflection point.

Based on the experimental results, a new interpretation of fatigue failure of CRM mixtures is proposed:

- At the beginning of the fatigue test, the CRM specimens showed a cement-dominated damage behaviour, followed by the breaking of the cementitious bonds, which led to the transition towards a bitumen-dominated damage behaviour. Afterwards, further damage of the bituminous bonds led to the specimen collapse.
- The inflection point of the DER curve was proposed to identify the failure of the cementitious bonds whereas, analogously to typical AC mixtures, the subsequent failure of the bituminous bonds was identified through the maximum phase angle value. Based on both criteria, a longer fatigue service life was observed for CRM specimen with lower cement content.

The findings of this research suggest that the fatigue failure of CRM mixtures during uniaxial laboratory tests is a composite phenomenon affected by both cementitious and bituminous bonds. However, it is still not clear how these mechanisms affect the field behaviour. Future work will also explore the possibility of applying the viscoelastic continuum damage (VECD) theory to CRM mixtures.

Funding

No funding was received for conducting this study.

Competing interests

The authors have no competing interests to declare that are relevant to the content of this article.

References

1. Wiesmeth, H., 2020. Implementing the circular economy for sustainable development. Elsevier. ISBN 9780128217986, https://doi.org/10.1016/C2019-0-04150-7.
2. Cross, S., Chesner, W., Justus, H., Kearney, E., 2011. Life-cycle environmental analysis for evaluation of pavement rehabilitation options. Transportation Research Record, 2227, pp. 43-52.
3. Giani, M.I., Dotelli, G., Brandini, N., Zampori, L., 2015. Comparative life cycle assessment of asphalt pavements using reclaimed asphalt, warm mix technology and cold in-place recycling. Resources, Conservation and Recycling, 104, pp. 224-238.
4. Thenoux, G., González, A., Dowling, R., 2007. Energy consumption comparison for different asphalt pavements rehabilitation techniques used in Chile. Resources, Conservation and Recycling, 49(4), pp. 325-339.
5. Thives, L.P., Ghisi, E., 2017. Asphalt mixtures emission and energy consumption: A review. Renewable and Sustainable Energy Reviews, 72, pp. 473-484.
6. Dołżycki, B., Jaskuła, P., 2019. Review and evaluation of cold recycling with bitumen emulsion and cement for rehabilitation of old pavements. Journal of Traffic and Transportation Engineering (English Edition), 6(4), pp. 311-323.

7. Dolzycki, B., Jaczewski, M., Szydlowski, C., 2017. The long-term properties of mineral-cement-emulsion mixtures. Construction and Building Materials, 156, pp. 799-808.
8. Godenzoni, C., Graziani, A., Bocci, E., Bocci, M., 2018. The evolution of the mechanical behaviour of cold recycled mixtures stabilised with cement and bitumen: field and laboratory study. Road Materials and Pavement Design, 19(4), pp. 856-877.
9. Guatimosim, F.V., Vasconcelos, K.L., Bernucci, L.L.B., Jenkins, K.J., 2018. Laboratory and field evaluation of cold recycling mixture with foamed asphalt. Road Materials and Pavement Design, 19(2), pp. 385-399.
10. Kuchiishi, A.K., Santos Antão, C.C.D., Vasconcelos, K., Bernucci, L.L.B., 2019. Influence of viscoelastic properties of cold recycled asphalt mixtures on pavement response by means of temperature instrumentation. Road Materials and Pavement Design, 20(sup2), pp. S710-S724.
11. Fedrigo, W., Núñez, W.P., Visser, A.T., 2020. A review of full-depth reclamation of pavements with Portland cement: Brazil and abroad. Construction and Building Materials, 262, 120540.
12. Fedrigo, W., Núñez, W.P., Schreinert, G.G., Kleinert, T.R., Matuella, M.F., Castañeda López, M.A., Ceratti, J.A.P., 2021. Flexural strength, stiffness and fatigue of cement-treated mixtures of reclaimed asphalt pavement and lateritic soil. Road Materials and Pavement Design, 22(5), pp. 1004-1022.
13. SABITA, 2020. Technical guideline: Bitumen stabilised materials. A Guideline for the Design and Construction of Bitumen Emulsion and Foamed Bitumen Stabilised Materials.
14. Orosa, P., Pérez, I., Pasandín, A.R., 2022. Evaluation of the shear and permanent deformation properties of cold in-place recycled mixtures with bitumen emulsion using triaxial tests. Construction and Building Materials, 328, 127054.
15. Bocci, M., Grilli, A., Cardone, F., Graziani, A., 2011. A study on the mechanical behaviour of cement-bitumen treated materials. Construction and Building Materials, 25(2), pp. 773–778.
16. Buczyński, P., Iwański, M., 2017. Fatigue Life Comparison of Recycled Cold Mixes with Foamed Bitumen and with Bitumen Emulsion. Procedia Engineering, 172, pp. 135-142.

17. Dolzycki, B., Szydlowski, C., Jaczewski, M., 2020. The influence of combination of binding agents on fatigue properties of deep cold in-place recycled mixtures in Indirect Tensile Fatigue Test (ITFT). Construction and Building Materials, 239, 117825.
18. Kavussi, A., Modarres, A., 2010. Laboratory fatigue models for recycled mixes with bitumen emulsion and cement. Construction and Building Materials, 24(10), pp. 1920–1927.
19. Leandri, P., Losa, M., Di Natale, A., 2015. Field validation of recycled cold mixes viscoelastic properties. Construction and Building Materials, 75, pp. 275–282.
20. Stimilli, A., Ferrotti, G., Graziani, A., Canestrari, F., 2013. Performance evaluation of a cold-recycled mixture containing high percentage of reclaimed asphalt. Road Materials and Pavement Design, 14(SUPPL.1), pp. 149–161.
21. Chelelgo, K., Gariy, Z.C.A., Shitote, S.M., 2019. Modeling of fatigue-strength development in cold-emulsion asphalt mixtures using maturity method. Applied Sciences, 9(13), 2694.
22. Ebels, L.-J., 2008. Characterisation of Material Properties and Behaviour of Cold Bituminous Mixtures for Road Pavements. PhD Dissertation, Stellenbosch University, South Africa.
23. Huang, W., Cao, M., Xiao, L., Li, J., Zhu, M., 2023. Experimental study on the fatigue performance of emulsified asphalt cold recycled mixtures. Construction and Building Materials, 369, 130607.
24. Di Benedetto, H., Perraton, D., Lamothe, S., Boussabnia, M.M., 2023. Rational relationship between the fatigue curves of asphalt mixes obtained from tension/compression and 4-point bending tests. Road Materials and Pavement Design, 24(sup1), pp. 192-208.
25. Di Benedetto, H., Partl, M.N., Francken, L., De La Roche Saint André, C., 2001. Stiffness testing for bituminous mixtures. Materials and Structures, 34(2), pp. 66-70.
26. Nemati, R., Dave, E.V., Sias, J.E., Thibodeau, E.S., Worsman, R.K., 2019. Evaluation of Laboratory Performance and Structural Contribution of Cold Recycled Versus Hot Mixed Intermediate and Base Course Asphalt Layers in New Hampshire. Transportation Research Record, 2673(6), pp. 467-476.

27. Tavassoti, P., Solaimanian, M., Chen, X., 2022. Characterization of fatigue performance of cold mix recycled asphalt mixtures through uniaxial tension-compression testing. Construction and Building Materials, 329, 127155.
28. EN 13043, 2002. Aggregates for bituminous mixtures and surface treatments for roads, airfields and other trafficked areas.
29. EN 13808, 2013. Bitumen and bituminous binders – Framework for specifying cationic bituminous emulsions.
30. EN 197-1, 2011. Cements – Part 1: Composition, specifications and conformity criteria for common cements.
31. Winter, M., Mollenhauer, K., Graziani, A., Mignini, C., Giancontieri, G., Lo Presti, D., Bjurström, H., Kalman, B., Hornych, P., Gaudefroy, V., 2020. Design of flexible pavements with cold recycled asphalt bases: Comparison of five national approaches. In: Proceedings of the 8th Transport Research Arena TRA 2020.
32. Mignini, C., Cardone, F., Graziani, A., 2022. Complex modulus of cement-bitumen treated materials produced with different reclaimed asphalt gradations. Materials and Structures, 55(7), 169.
33. Spadoni, S., Ingrassia, L.P., Jaskuła, P., Canestrari, F., 2023. Advanced fatigue and rutting characterisation of Polish asphalt mixtures based on the VECD model and viscoplastic shift model. Road Materials and Pavement Design, 24(S1), pp. 145-159.
34. Graziani, A., Raschia, S., Mignini, C., Carter, A., Perraton, D., 2020. Use of fine aggregate matrix to analyze the rheological behavior of cold recycled materials. Materials and Structures, 53(4), 72.
35. EN 12697-31, 2019. Bituminous mixtures – Test methods – Part 31: Specimen preparation by gyratory compactor.

36. Grilli, A., Graziani, A., Bocci, E., Bocci, M., 2016. Volumetric properties and influence of water content on the compactability of cold recycled mixtures. Materials and Structures, 49, pp. 4349-4362.

37. Cardone, F., Grilli, A., Bocci, M., Graziani, A., 2014. Curing and temperature sensitivity of cement–bitumen treated materials, International Journal of Pavement Engineering, 16(10), pp. 868-880.

38. EN 12697-6, 2020. Bituminous mixtures – Test methods – Part 6: Determination of bulk density of bituminous specimens.

39. EN 12697-8, 2018. Bituminous mixtures – Test methods – Part 8: Determination of void characteristics of bituminous specimens.

40. AASHTO PP 99, 2019. Standard Practice for Preparation of Small Cylindrical Performance Test Specimens Using the Superpave Gyratory Compactor (SGC) or Field Cores.

41. AASHTO T 400, 2023. Standard method of test for determining the damage characteristic curve and failure criterion using the Asphalt Mixture Performance Tester (AMPT) cyclic fatigue test.

42. Underwood, B.S., Kim, Y.R., Guddati, M.N., 2010. Improved calculation method of damage parameter in viscoelastic continuum damage model. International Journal of Pavement Engineering, 11(6), pp. 459–476.

43. Jaczewski, M., Szydlowski, C., Dolzycki, B., 2022. Preliminary study of linear viscoelasticity limits of cold recycled mixtures determined in Simple Performance Tester (SPT). Construction and Building Materials, 357, 129432.

44. Jaczewski, M., Szydłowski, C., Dołżycki, B., 2023. Stiffness of cold-recycled mixtures under variable deformation conditions in the IT-CY test. Case Studies in Construction Materials, 18, e02066.

45. Bhasin, A., Castelo Branco, V.F., Masad, E., Little, D.N., 2009. Quantitative comparison of energy methods to characterize fatigue in asphalt materials. Journal of Materials in Civil Engineering, 21(2), pp. 83–92.
46. Gajewski, M., Bańkowski, W., Pronk, A.C., 2020. Evaluation of fatigue life of high modulus asphalt concrete with use of three different definitions. International Journal of Pavement Engineering, 21(14), pp. 1717-1728.
47. Shen, S., Lu, X., 2011. Energy based laboratory fatigue failure criteria asphalt materials. Journal of Testing and Evaluation, 39(3), 103088.
48. Sudarsanan, N., Kim, Y.R., 2022. A critical review of the fatigue life prediction of asphalt mixtures and pavements. Journal of Traffic and Transportation Engineering (English Edition), 9(5), pp. 808-835.
49. AASHTO T 321, 2017. Standard method of test for determining the fatigue life of compacted asphalt mixtures subjected to repeated flexural bending.
50. EN 12697-24, 2018. Bituminous mixtures – Test methods – Part 24: Resistance to fatigue.
51. Reese, R., 1997. Properties of aged asphalt binder related to asphalt concrete fatigue life. Journal of the Association of Asphalt Paving Technologists, 66, pp. 604-632.
52. Pronk, A.C. and Hopman, P.C., 1991. Energy dissipation: the leading factor of fatigue. In: Highway Research: Sharing the Benefits. Thomas Telford Publishing, London, pp. 255-267.
53. Van Dijk, W., 1975. Practical Fatigue Characterization of Bituminous Mixes. Proceedings of the Association of Asphalt Paving Technologists (AAPT), 44, pp. 38–74.
54. Van Dijk, W., Visser, W., 1977. The Energy Approach to Fatigue for Pavement Design. Proceedings of the Association of Asphalt Paving Technologists (AAPT), 46, pp. 1–40.
55. Monismith, C.L., Deacon, J.A., 1969. Fatigue of asphalt paving mixtures. Transportation Engineering Journal of ASCE, 95(2), pp. 317-346.
56. Di Benedetto, H., De La Roche, C., Baaj, H., Pronk, A., Lundström, R., 2004. Fatigue of bituminous mixtures. Materials and Structures, 37(267), pp. 202-216.

57. Lee, K.C., 2020. Improvement in dynamic modulus and cyclic fatigue testing of asphalt mixture. PhD Thesis, North Carolina State University.

58. Virgili, A., Canestrari, F., Grilli, A., Santagata, F.A., 2009. Repeated load test on bituminous systems reinforced by geosynthetics. Geotextiles and Geomembranes, 27(3), pp. 187-195.

59. Tapsoba, N., Sauzéat, C., Di Benedetto, H., 2013. Analysis of fatigue test for bituminous mixtures. Journal of Materials in Civil Engineering, 25(6), pp. 701-710.